Molecular Therapy
Original Article

CANT1 lncRNA Triggers Efficient Therapeutic Efficacy by Correcting Aberrant lncing Cascade in Malignant Uveal Melanoma

Yue Xing,[1,2] Xuyang Wen,[1,2] Xia Ding,[1,2] Jiayan Fan,[1,2] Peiwei Chai,[1,2] Renbing Jia,[1] Shengfang Ge,[1] Guanxiang Qian,[1] He Zhang,[1] and Xianqun Fan[1]

[1]Department of Ophthalmology, Ninth People's Hospital, Shanghai JiaoTong University School of Medicine, Shanghai 200025, P.R. China

Uveal melanoma (UM) is an intraocular malignant tumor with a high mortality rate. Recent studies have shown the functions of long non-coding RNAs (lncRNAs) in tumorigenesis; thus, targeting tumor-specific lncRNA abnormalities has become an attractive approach for developing therapeutics to treat uveal melanoma. In this study, we identified a novel nuclear *CANT1* lncRNA (*CASC15-New-Transcript 1*) that acts as a necessary UM suppressor. *CANT1* significantly reduced tumor metastatic capacity and tumor formation, either in cell culture or in animals harboring tumor xenograft. Intriguingly, *XIST* lncRNA serves as a potential target of *CANT1*, and *JPX* or *FTX* lncRNA subsequently serves as a contextual hinge to activate a novel *CANT1-JPX/FTX-XIST* long non-coding (lncing) pathway in UM. Moreover, *CANT1* triggers the expression of JPX and FTX by directly binding to their promoters and promoting H3K4 methylation. These observations delineate a novel lncing cascade in which lncRNAs directly build a lncing cascade without coding genes that aims to modulate UM tumorigenesis, thereby specifying a novel "lncing-cascade renewal" anti-tumor therapeutic strategy by correcting aberrant lncing cascade in uveal melanoma.

INTRODUCTION

Uveal melanoma (UM) is a special type of melanoma that originates in the uvea of the eye and is the most common intraocular malignant tumor in adults.[1,2] In the past decade, most studies have focused on the mechanisms underlying UM tumorigenesis by identifying chromosomal and/or genomic abnormalities. For instance, the loss of one copy of chromosome 3 has been identified as the most frequent event in UM.[3,4] As early events, some mutations in *GNAQ* or *GNA11* result in marked promotion of cell proliferation and sensitize cells to mitogen-activated protein kinase (MAPK) inhibitors.[5] In addition, it has been reported that the mutations found in *BAP1* are strongly associated with increased metastasis. In contrast, mutations in *SF3B1* or *EIF1AX* have been associated with good prognosis.[5] Theoretically, the tumorigenesis is a multistep process involving genetic and epigenetic alterations. We thus were interested in shedding light on the epigenetic mechanisms underlying UM progression.

Epigenetics is the study of physiological traits that are inherited by daughter cells without changes in DNA sequence.[6] Epigenetic research mainly includes the regulation of non-coding RNAs, the modification of histone methylation, and conformational changes in the chromosomes.[7] An increasing number of studies in various fields have particularly focused on the function of long non-coding RNAs (lncRNAs). For example, we previously reported that the *Kcnq1ot1* lncRNA regulates *Kcnq1* imprinting by orchestrating a long-range intrachromosomal loop.[8] The *RoR* lncRNA can modulate pluripotency and self-renewal in induced pluripotent stem cell (iPSC) induction.[9] Recent findings have also implicated lncRNAs in several of the steps leading to cancer development. For instance, the *MALAT1* lncRNA is a highly conserved lncRNA that participates in tumor proliferation, migration, and invasion in many common cancers.[10–12] We recently also showed that *ROR* lncRNA blocks the binding of histone methyltransferase G9A to its target gene and promotes tumorigenesis.[13] Thus, the orchestrating roles of lncRNA raise the hypothesis that correction of lncRNA-guided abnormalities has become an attractive strategy in control the malignancy of UM.

In this study, we successfully identified a novel lncRNA, named *CASC15-New-Transcript 1* (*CASC15-NT1* or *CANT1*), that functions as a necessary non-coding UM suppressor. We previously improved the anti-tumor effect using a "double-targeted" and "domino-effect-like" therapeutic strategy.[14,15] Thus, we further propose an "lncing-cascade renewal" therapeutic strategy that corrects aberrant lncing (long non-coding) cascade. This preclinical study delineates the role of *CANT1* in malignant UM and demonstrates that our novel therapy significantly enhanced anti-tumor efficiency.

Received 27 October 2016; accepted 25 February 2017;
http://dx.doi.org/10.1016/j.ymthe.2017.02.016.

[2]These authors contributed equally to this work.

Correspondence: He Zhang, PhD, Ninth People's Hospital, Shanghai JiaoTong University School of Medicine, Shanghai, 200025, P.R. China.
E-mail: zhanghe@sjtu.edu.cn
Correspondence: Xianqun Fan, MD, PhD, Ninth People's Hospital, Shanghai JiaoTong University School of Medicine, Shanghai, 200025, P.R. China.
E-mail: drfanxianqun@126.com

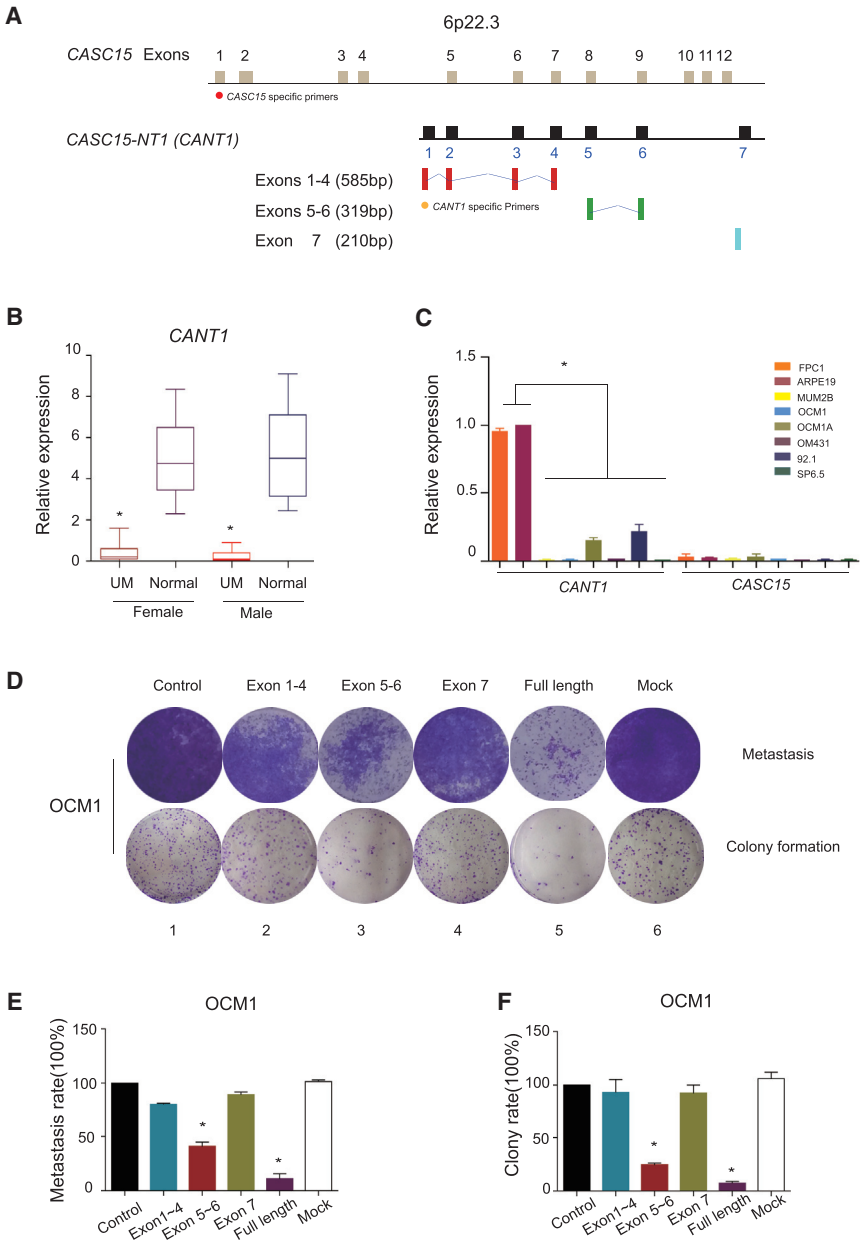

Figure 1. Identification of the Novel *CANT1* lncRNA

(A) Genomic structure of *CANT1*. The gray and black rectangles indicate the exons of CASC15 and *CANT1*, respectively. The red rectangles indicate exons 1–4 of *CANT1*. The green rectangles indicate exons 5 and 6 of *CANT1* (*CANT1*). The blue rectangle indicates the last exon of *CANT1*. (B) Real-time PCR examination of *CANT1* expression in UM tissues (n = 17). Normal uveal tissues (n = 12) were used as control. The relative values are normalized to the *GAPDH* expression level and are presented as mean ± SEM. *p < 0.05. (C) Expression of *CASC15* and *CANT1* in six UM cell lines: 92.1, OCM1A, OCM1, MUM2B, OM431, and SP6.5. ARPE19 and FPC cells were used as a normal control, and isoform-specific primers were used. The value obtained for the ARPE19 control group was set to 100%. Data are presented as mean ± SEM. *p < 0.05. (D) A transwell assay was performed to evaluate the migration ability of OCM1 cells expressing different domains of *CANT1*. A colony formation assay was performed to assess the tumor growth of OCM1 cells expressing different domains of *CANT1*. Wild-type OCM1 cells were used as a control. Mock, cell colonies that expressed an empty vector. (E) The absorbance values at a wavelength of 630 nm of stained migrated cells at day 3 were obtained to calculate the metastasis rate. The value obtained for the control group was set to 100%. All of the experiments were performed in triplicate, and the relative metastasis rates are shown as mean ± SEM. *p < 0.05. (F) Quantification of visible colonies. The colony number of the control group was set to 100%. All of the experiments were performed in triplicate, and the relative colony formation rates are shown as mean ± SEM. *p < 0.05.

RESULTS

The Novel CASC15-NT1 lncRNA Contributes to UM Progression

To investigate the roles of lncRNAs in UM, we first focused on the susceptibility chromosome 6p22.3 locus, where the candidate *CASC15* lncRNA (formerly called *LINC00340*) was shown to be involved in the tumorigenesis process of many cancers, except for UM.[16–18] As detailed in the University of California, Santa Cruz (UCSC), and National Center for Biotechnology Information (NCBI) databases, the *CASC15* lncRNA is 1,904 bp in length, with 12 exons, and is located at 6p22.3 (Figure 1A, gray box). Given this information, we next determined whether the previously reported *CASC15* transcript exists in UM. However, after rapid amplification of cDNA ends (RACE) detection, we found a novel 1,114 bp transcript spanning 7 exons (Figure S1A; Table S1) in normal human uveal tissues. More precisely, exons 2–6 were consistent with the predicted exons 5–9, whereas exons 1 and 7 were located on the predicted intron 4 and 3′ UTR, respectively (Figure 1A, black box). Using the GENCODE annotation of the human genome,[19,20] we then confirmed the absence of coding evidence for this novel transcript. Collectively, these data show that this novel isoform of the *CASC15* lncRNA is a non-coding transcript identified in UM, and we therefore named it *CASC15-New-Transcript 1* (*CASC15-NT1* or *CANT1*; GenBank: KP981381.1).

To evaluate the clinical relevance of CANT1, we then examined the expression of CANT1 in our cohort of Chinese UM tissue samples from 12 female and 5 male subjects. As expected, CANT1 expression was significantly reduced in these samples compared with that detected in a normal cohort consisting of 7 female and 5 male subjects. We then detected whether the CANT1 expression of normal tissues

was presented in a gender-specific manner, but there was no significant variation between normal male and female tissues (Figure 1B; Table S2).Because of the significant overlap between the CASC15 and CANT1 lncRNAs, we then designed isoform-specific qPCR primers to detect their expression in UM cell lines (Figure 1A, red and yellow circles). As expected, we found that both the CASC15 and CANT1 lncRNAs presented very weak expression in UM cells (Figure 1C). Next, in the normal male and female cells, we detected significantly high expression of CANT1 (Figure 1C, first and second columns). However, the CASC15 retained low expression in normal cells (Figure 1C, ninth column). These data indicate that this novel CANT1 is alternative-spliced from chromosome 6p22.3 and is likely to play unknown role in UM tumorigenesis.

To decipher the functional role and key regulatory domain of this novel transcript in tumorigenesis, we then established four expression plasmids containing either the full-length sequence (1,114 bp) or shorter fragments, namely exons 1–4 (585 bp), exons 5–6 (319 bp), and exon 7 (210 bp) (Figure 1A). These plasmids were then packaged into a lentivirus and transfected into OCM1 cells. As expected, all four plasmids were successfully stably expressed in OCM1 cell lines (Figure S1B). We then determined which domain contributes to tumor migration and formation. In OCM1 cells, the fragments consisting of exons 1–4 (Figure 1D, upper lane 2) and exon 7 (Figure 1D, upper lane 4) produced a slight decrease in tumor migration, whereas the fragment consisting of exons 5 and 6 (Figure 1D, upper lane 3) and the full-length lncRNA (Figure 1D, upper lane 5) significantly inhibited cell migration. A statistical analysis revealed that the metastatic rate observed after the overexpression of full-length *CANT1* decreased sharply to 25% in OCM1 cells. Similarly, OCM1 cells enriched in exons 5 and 6 showed an approximate 60% reduction in metastasis (Figure 1E). As determined through cell colony formation assay, OCM1 cells expressing either the fragment consisting of exons 1–4 (Figure 1D, bottom lane 2) or the fragment consisting of exon 7 (Figure 1D, bottom lane 4) showed a minimal reduction, whereas the OCM1 cells expressing exons 5 and 6 (Figure 1D, bottom lane 3) or the full-length sequence (Figure 1D, bottom lane 5) displayed markedly strong suppression of tumor formation. Similarly, a statistical analysis also confirmed that either the fragment containing exons 5 and 6 or the full-length sequence resulted in significant inhibition of tumor formation (Figure 1F). These results demonstrate that *CANT1* serves as a tumor suppressor by modulating tumor formation and metastasis in UM, and a small fragment containing exons 5 and 6 of *CANT1* (*CANT1-S*) constitutes a functional domain that contributes to UM tumorigenesis.

CANT1 Modulates UM Tumorigenesis In Vitro and In Vivo

Next, to avoid non-physiological overexpression may force glorious phenomenon, we selected the colonies that presented close to 3-fold overexpression of both *CANT1* and *CANT1-S* (Figures S2A and S2B) and investigated whether *CANT1* and *CANT1-S* could regulate tumorigenesis in two UM cell lines. Using a classical transwell assay, we compared parental (Figure 2A, upper lane 1) and mock-transfected (empty vector) MUM2B control cells (Figure 2A, upper lane 4) with *CANT1*-expressing and *CANT1-S*-expressing MUM2B cells and found that the cells expressing *CANT1* and *CANT1-S* showed significantly weaker migratory ability (Figure 2A, upper lanes 2 and 3). A statistical analysis revealed that the metastatic rate of MUM2B cells after *CANT1* overexpression decreased sharply to 30% (Figure 2B, left). Moreover, the *CANT1-S*-enriched MUM2B cells showed an approximately 60% reduction in metastasis (Figure 2B, left). Similarly, the *CANT1*-expressing and *CANT1-S*-expressing OCM1 cells showed marked inhibition of tumor metastasis (Figure 2B, right).

We then investigated the ability of *CANT1* and *CANT1-S* to suppress tumor formation in UM cells in vitro through a soft agar assay. As expected, we found a significantly smaller number of visible colonies of *CANT1*-enriched and *CANT1-S*-enriched UM cells (Figure 2C, lanes 2 and 3). Colony quantification showed that the rate of colony formation was reduced to almost 40% in two UM cell lines (Figure 2D). To examine the ability of *CANT1* to suppress tumor formation in vivo, we established a xenograft model of nude mice using *CANT1-S*-enriched MUM2B cells and untreated MUM2B cells. Compared with the control group, tumor growth was significantly reduced in the animals carrying cells presented enriched expression of the *CANT1-S* lncRNA ($n = 5$, $^*p < 0.05$; Figure 2E). These data further indicated that *CANT1* could modulate UM progression in vivo.

XIST Functions as the Potential Downstream Target of the CANT1 lncRNA

To explore the *CANT1*-mediated mechanism underlying tumorigenesis, we searched for the key regulatory targets of *CANT1*. We performed a genome-wide cDNA array comparing *CANT1*-enriched and parental control cells belonging to both the MUM2B and OCM1 UM cell lines (Gene Expression Omnibus: GSE71161). As expected, we found eight genes that presented strong alterations in expression (with fold changes > 2) in both cell lines (Figure 3A). Intriguingly, the gene presented the most robust change in expression was *XIST* (X-inactive specific transcript) (Figure 3B), which is not a coding gene but a well-known female-specific lncRNA that participates in X chromosome inactivation (XCI),[21] sparking our interest in exploring its role in UM tumorigenesis.

Considering that *XIST* is a female-specific lncRNA, we examined the gender origin of UM cells. *SRY* (sex-determining region Y) and *DYS14* (also TSPY1, testis-specific protein Y-linked 1) are classical markers for gender identification,[22–24] which are located on the Y chromosome and detectable only in male genome DNA. Through PCR with genome DNA of UM cells, *SRY* and *DYS14* markers were detectable in male-derived ARPE19 control cells (from the ATCC website; Figure 3C, lane 1) and absent in female-derived primary positive control cells (FPC1; obtained from female uveal tissue through primary culture) (Figure 3C, lane 2). Both *SRY* and *DYS14* did not exist in MUM2B and OCM1 cells, indicating that these two cell lines originated from female donors (Figure 3C, lanes 3 and 4). In addition, in female FPC cells, *XIST* was highly expressed compared with the male-derived ARPE19 negative control cells. However, in MUM2B and OCM1 tumor cells, we failed to detect *XIST* expression in these

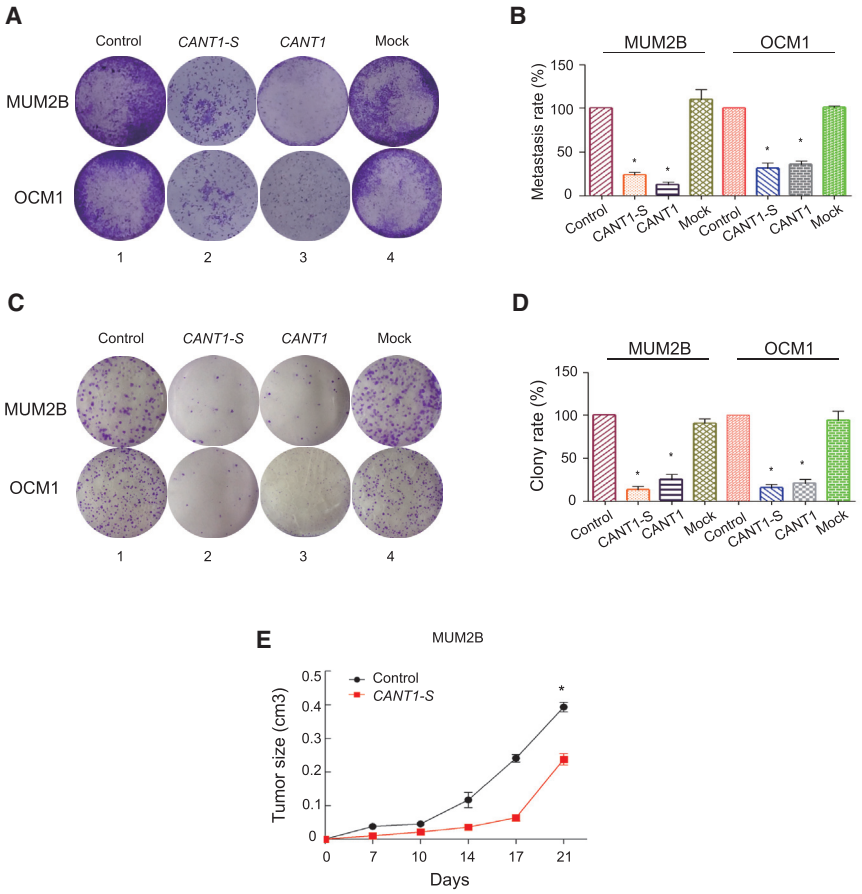

Figure 2. Functional Roles of the *CANT1* lncRNA in UM

(A and B) Migration ability of MUM2B and OCM1 cells in a transwell assay. (A) Images of the cells on the outer side of the transwell. Control, wild-type UM cells. Mock, cell colonies that expressed an empty vector. *CANT1* indicates cells expressing the full-length *CANT1* lncRNA. *CANT1-S* indicates cells expressing the fragment consisting of exons 5 and 6 of the *CANT1* lncRNA. (B) The absorbance values at a wavelength of 630 nm of stained migrated cells at day 3 were obtained to calculate the metastasis rate. The value of the control group was set to 100%. All of the experiments were performed in triplicate, and the relative metastasis rates are shown as mean ± SEM. *$p < 0.05$. (C and D) Tumorigenicity was determined through a soft agar in vitro assay. (C) Images of the cell colonies in the upper layer of soft agar. (D) Quantification of visible colonies. The colony number in the control group was set to 100%. All of the experiments were performed in triplicate, and the relative colony formation rates are shown as mean ± SEM. *$p < 0.05$. (E) The tumorigenesis ability was determined using a xenograft in vivo assay model. Four-week-old male nude mice were used in this assay (n = 5). The tumor sizes were calculated using the formula length × width × width/2 and are presented as mean ± SEM. *$p < 0.05$.

two control UM cell lines (Figure 3D). We then examined whether *XIST* expression was increased in *CANT1*-expressing cells. As expected, *XIST* expression was significantly increased in both UM cell lines after *CANT1* overexpression (Figure 3D). Moreover, using RNA fluorescence in situ hybridization (RNA-FISH) experiment, we found that *XIST* formed a cloudlike structure in normal female cells (Figure 3E, upper lanes 1–3), but *XIST* showed highly dispersed organization in *CANT1*-expressed UM cells (Figure 3E, bottom, lanes 2 and 4), suggesting that *XIST* is likely to merely express but does not trigger XCI at this stage.

To determine the clinical relevance of *XIST* in UM, we collected human UM tissue samples (Table S2) to examine *XIST* expression. The expression of *XIST* was markedly reduced in both female (n = 12) and male (n = 7) UM tissues, and no significant difference was found between female and male UM tissues (Figure 3F), suggesting that UM tumorigenesis is only loosely associated with gender. These data suggest that the *XIST* lncRNA may represent a potential target of the *CANT1* lncRNA and deserves further analysis.

The JPX and FTX lncRNAs Are Required for XIST Activation in UM

XIST is a classic lncRNA that plays a key role in XCI. We therefore examined which factors involved in XCI are required for *XIST* activation in UM. Because the *JPX*, *FTX*, and *TSIX* lncRNAs have been demonstrated to regulate *XIST* activation, we first assessed their expression in UM. Real-time PCR results showed that *JPX* expression was extremely weak in UM cells, whereas *JPX* expression was significantly increased in *CANT1*-expressing cells (Figure 4A). Similarly, after *CANT1* overexpression, *FTX* expression was markedly enhanced compared with that in control UM cells (Figure 4B). Intriguingly, *TSIX* was not expressed in UM cells, and its expression remained unaffected, regardless of the *CANT1* expression status (Figure S3A), suggesting that *JPX* and *FTX* but not *TSIX* could act downstream of *CANT1* and might participate in *CANT1*-mediated *XIST* regulation in UM.

On the basis of this information, we explored whether *JPX* or *FTX* could directly modulate *XIST* expression in UM. We used the classic RNAi method to knock down *JPX* expression in *CANT1*-enriched UM cells (Figures S3B and S3C). As expected, a real-time PCR examination revealed that the reactivation of *XIST* expression was markedly inhibited by *JPX* silencing compared with the levels found in *CANT1*-expressing cells and the non-transfected control without *CANT1* (Figure 4C, left, *CANT1*+si*JPX* column). In addition, we also demonstrated that *XIST* expression was significantly decreased in *CANT1*-enriched MUM2B cells after *FTX* silencing (Figure 4C, left, *CANT1*+si*FTX* column). Similarly, we also observed this phenomenon in *CANT1*-enriched OCM1 cells after the silencing of *JPX* or *FTX* (Figure 4C, right). These data suggest that either *JPX* or *FTX* could regulate *XIST* expression and likely serves as a

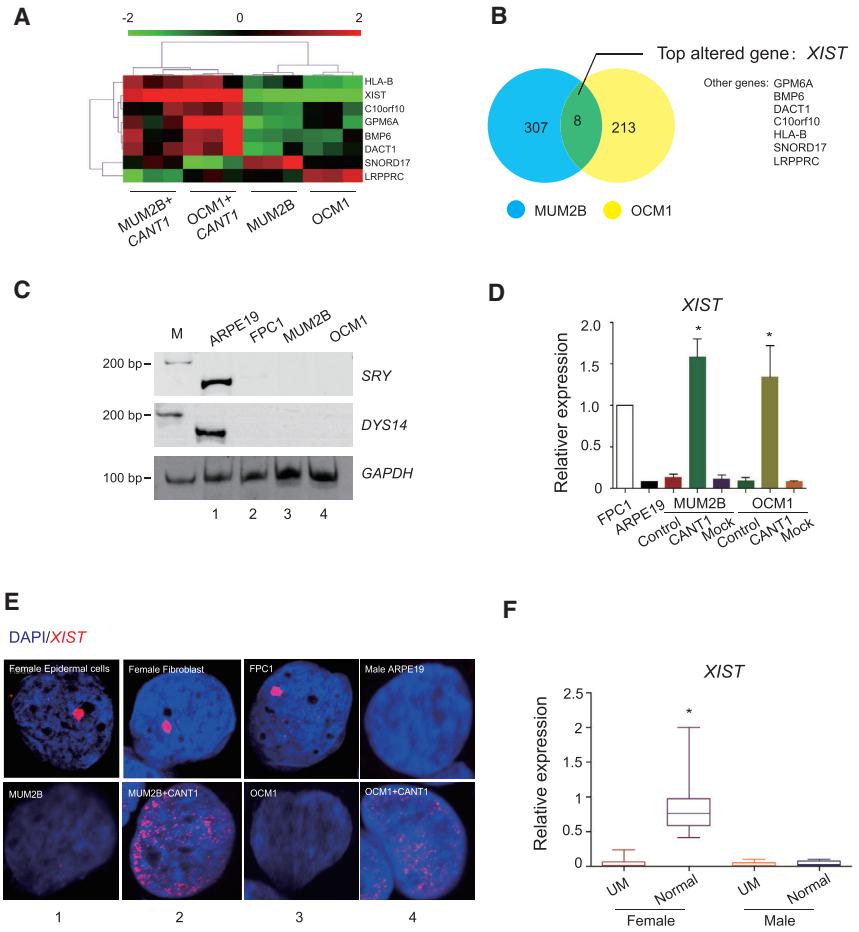

Figure 3. Regulatory Targets of *CANT1* lncRNA in UM

(A) Heatmap of differentially expressed genes. Genes presenting a 2-fold change in expression between *CANT1*-overexpressing and control MUM2B and OCM1 cells, as determined through a genome-wide cDNA array, are shown. (B) The overlapping genes presenting altered expression between the two UM cell lines are shown, and the eight altered genes are shown. (C) The existence of the *SRY* and *DYS14* markers, which are located on the Y chromosome, was determined by PCR with genomic DNA. Male (APRE19) and female (FPC1) cells served as the positive and negative controls for gender identification. FPC1 cells were obtained from female uveal tissue through primary culture. (D) Validation of the *XIST* microarray data by real-time PCR and assessment of the expression of *XIST* in APRE19 and FPC1 cells. The values are normalized to the *GAPHD* expression level and are presented as mean ± SEM. *$p < 0.05$. The value obtained for normal female cells was set to 1. (E) Representative FISH images showing staining of DAPI (blue) and *XIST* (red) in cells. The scale bars represent 5 μm. (F) Real-time PCR examination of *XIST* expression in UM tissues (12 female and 5 male subjects). Normal uveal tissues (7 female and 5 male subjects) were used as a control. The relative values were normalized to the *GAPDH* expression level and are presented as mean ± SEM. *$p < 0.05$.

contextual hinge to activate the *CANT1*-mediated lncing cascade in UM formation.

A lncing Cascade Is Triggered by CANT1 in UM Cells

To further confirm the epistatic relationships among these lncRNAs in the *CANT1*-guided lncing cascade as well as the aforementioned effects of *JPX* or *FTX* knockdown, we also silenced *XIST* expression (Figures S3C and S3D). As expected, *CANT1* expression in *CANT1*-enriched MUM2B cells was not affected by *XIST* silencing (Figure 4D, left, *CANT1*+si*XIST* column). Similarly, we obtained consistent results in *CANT1*-enriched OCM1 cells (Figure 4D, right, *CANT1*+si*XIST* column). These data suggest that *CANT1* is the actual upstream trigger of the lncing cascade regulating UM progression. Additionally, we found that the expression of either *JPX* (Figure S4A, *CANT1*+si*XIST* column) or *FTX* (Figure S4B, *CANT1*+si*XIST* column) remained unaltered following *XIST* knockdown, indicating that *JPX* or *FTX* could act upstream of *XIST* expression. Intriguingly, *JPX* expression was not influenced by *FTX* silencing (Figure S4A, *CANT1*+si*FTX* column), and conversely, *FTX* expression was unaffected in *JPX*-deficient UM cells (Figure S4B, *CANT1*+si*JPX* column). Taken together, these data demonstrated that *CANT1* modulates UM tumorigenesis via a novel independent *CANT1-JPX/FTX-XIST* lncing pathway (Figure 4E).

The CANT1-Guided lncing Cascade Is Required for UM Tumorigenesis

To explore whether the *CANT1*-guided lncing cascade is required for UM formation, we then disrupted this cascade by silencing the expression of each key lncRNA: *JPX*, *FTX*, and *XIST*. As expected, we found that the migratory ability of UM cells was markedly inhibited after *CANT1* overexpression (Figure 5A, lane 2) compared with that of control UM cells (Figure 5A, lane 1), re-confirming that *CANT1* acts as a tumor suppressor. We then examined the role of *JPX* in UM metastasis via *JPX* silencing. Similar to *CANT1*, *JPX* was not expressed in MUM2B and OCM1 cells, but its expression was reactivated after *CANT1* overexpression, as shown in Figure 4A. Therefore, we used *CANT1*-enriched UM cells to assess the functional role of *JPX* silencing. As expected, the migratory ability of the tumor cells was partially restored by the silencing of activated *JPX* lncRNA in *CANT1*-enriched tumor cells (Figure 5A, lane 3). Similarly, *FTX* expression was also reactivated in *CANT1*-enriched cells (Figure 5A, lane 4), and upon *FTX* knockdown, the metastatic potential of *CANT1*-expressing tumor cells was partially restored compared with that of the negative control cells (Figure 5A, lane 6). In addition, the silencing of *XIST* in *CANT1*-enriched cells partially restored the migration capacity of these cells (Figure 5A, lane 5). Furthermore, through an in vitro colony formation assay, we found that the colony-forming ability of *CANT1*-enriched UM cells was significantly reduced (Figure 5C, lane 2). In addition, after silencing any of the three downstream lncRNAs (*JPX*, *FTX*, or *XIST*), the *CANT1*-enriched UM tumor cells partially restored their colony-forming ability (Figure 5C, lanes 3–5) compared with the controls

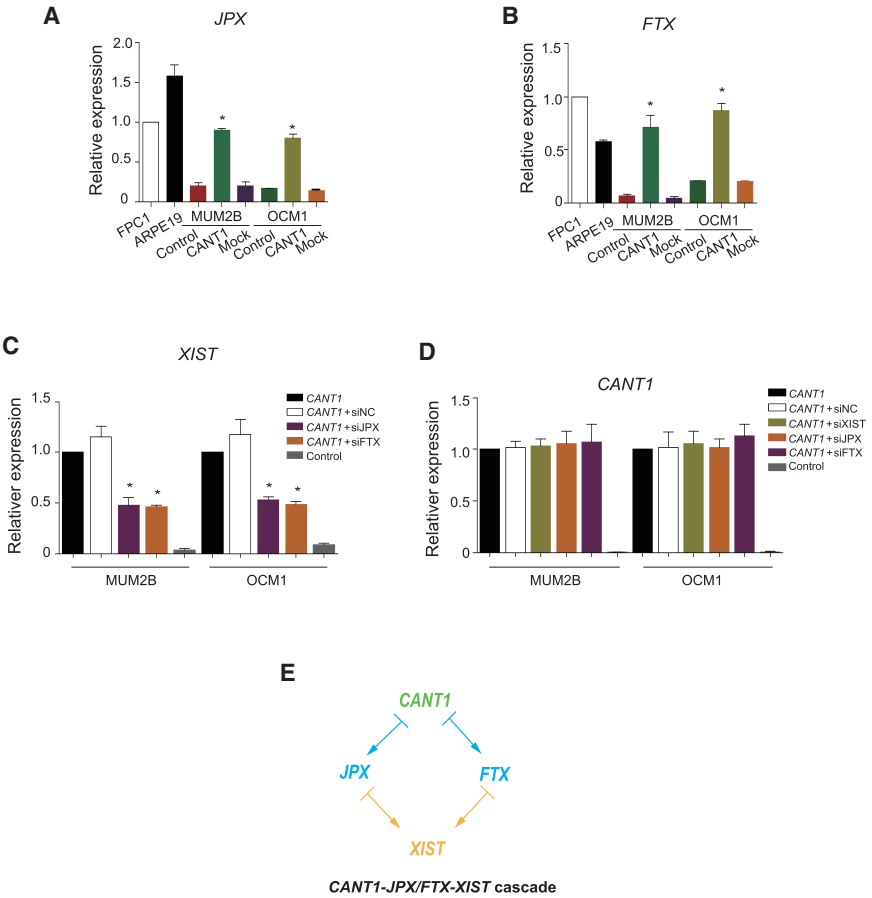

Figure 4. Novel *CANT1*-Guided Cascade in UM

(A) The expression of *JPX* was examined by real-time PCR. FPC1 cells served as the female control, and APRE19 cells were used as the male control. Data are presented as mean ± SEM. *$p < 0.05$. (B) Real-time PCR quantification of *FTX* expression in UM cells. The value of FPC1 cells was set to 1. Data are presented as mean ± SEM. *$p < 0.05$. (C) Real-time PCR examination of *XIST* expression after siRNA-guided knockdown in *CANT1*-expressing UM cells, including MUM2B and OCM1 cells. *CANT1*, untreated *CANT1*-expressing cells; *CANT1*+siNC, siNC-treated *CANT1*-expressing cells; control, untreated UM cells. (D) Quantification of *CANT1* expression in different siRNA-treated *CANT1*-expressing UM cells, including MUM2B and OCM1 cells. The value of untreated *CANT1* cells was set to 1. Data are presented as mean ± SEM. *$p < 0.05$. (E) Schematic of the *CANT1*-guided cascade.

(Figure 5C, lanes 2 and 6). A statistical analysis of quantified data also confirmed the aforementioned conclusions (Figures 5B and 5D). The obtained data demonstrate that the *CANT1*-guided lncing cascade involving *JPX*, *FTX*, and *XIST* acts as a tumor-suppressor cascade and is required for the progression of UM tumorigenesis. To determine the clinical relevance of the *CANT1*-guided cascade in UM, we collected human UM tissue samples (Table S2) and examined the expression of the cascade participants in these samples. As expected, the expression of *JPX* and *FTX* lncRNAs (Figures 5E and 5F) were also markedly reduced in UM tissues. These data may support the clinical relevance of the *CANT1*-guided non-coding cascade in UM tumorigenesis.

CANT1 Directly Binds to the JPX and FTX Promoters

Because *JPX* and *FTX* were found to act as critical mediators of two pathways in the *CANT1*-guided cascade (*CANT1-JPX-XIST* and *CANT1-FTX-XIST*, respectively), we then examined the role of *CANT1* in regulating their expression. Using the *U2* non-coding RNA (ncRNA) as a positive control (Figure 6A, panel 3, lane 2), we found that *CANT1* was located mainly in the nucleus in MUM2B cells (Figure 6A, panel 1, lane 2). Similarly, *CANT1* was also located in the nucleus of OCM1 cells (Figure 6A, panel 1, lane 5). These data suggested that *CANT1* is a novel nuclear lncRNA and might guide this lncing cascade via a nuclear, chromosome-related mechanism. To explore this possibility, we used classical chromatin oligonucleotide precipitation (ChOP). Using a diagram, we designed a biotin-labeled, short oligonucleotide aligned with *CANT1*. Sites a and c were used to detect the promoter regions of *JPX* and *FTX*, respectively, and sites b and d were found to serve as non-specific promoter regions (Figure 6B). After pull-down, we found that *CANT1* can more strongly bind to the *JPX* promoter in two UM cell lines (Figures 6C and 6D, site a, left, *CANT1* column), whereas this DNA-RNA interaction was not observed in the parental or mock-transfected control cells (Figure 6C, site a, right). We also performed real-time qPCR to examine the interaction of the short fragment *CANT1-S* and the *JPX* promoter. As expected, we found that *CANT1-S* interacted with the *JPX* promoter in both *CANT1-S*-enriched MUM2B (Figure 6C, site a, left, *CANT1-S* column) and OCM1 cells (Figure 6D, site a, left, *CANT1-S* column), whereas a negative oligonucleotide control that was not aligned with *CANT1-S* did not present lncRNA-DNA binding in both cell lines (Figures 6C and 6D, right). Similarly, we also detected interactions between *CANT1* RNA and the *FTX* promoter in *CANT1*-enriched MUM2B and OCM1 cells (Figures 6E and 6F, site c, left, *CANT1* column) compared with the controls (Figures 6E and 6F, site c, right, and site d). In addition, we also confirmed that the *CANT1-S* lncRNA bound to the *FTX* promoter region in both MUM2B (Figure 6E, site c, left, *CANT1-S* column) and OCM1 cells (Figure 6F, site c, left, *CANT1-S* column). Taken together, these results demonstrate that either full-length *CANT1* or the short fragment *CANT1-S* might regulate *JPX* and *FTX* expression by binding to key DNA regulatory regions in their promoters.

CANT1 Modulates JPX and FTX Expression by Activating Histone H3K4 Methylation

We then explored whether epigenetic modifications were altered by *CANT1* binding and whether the histone methylation status was

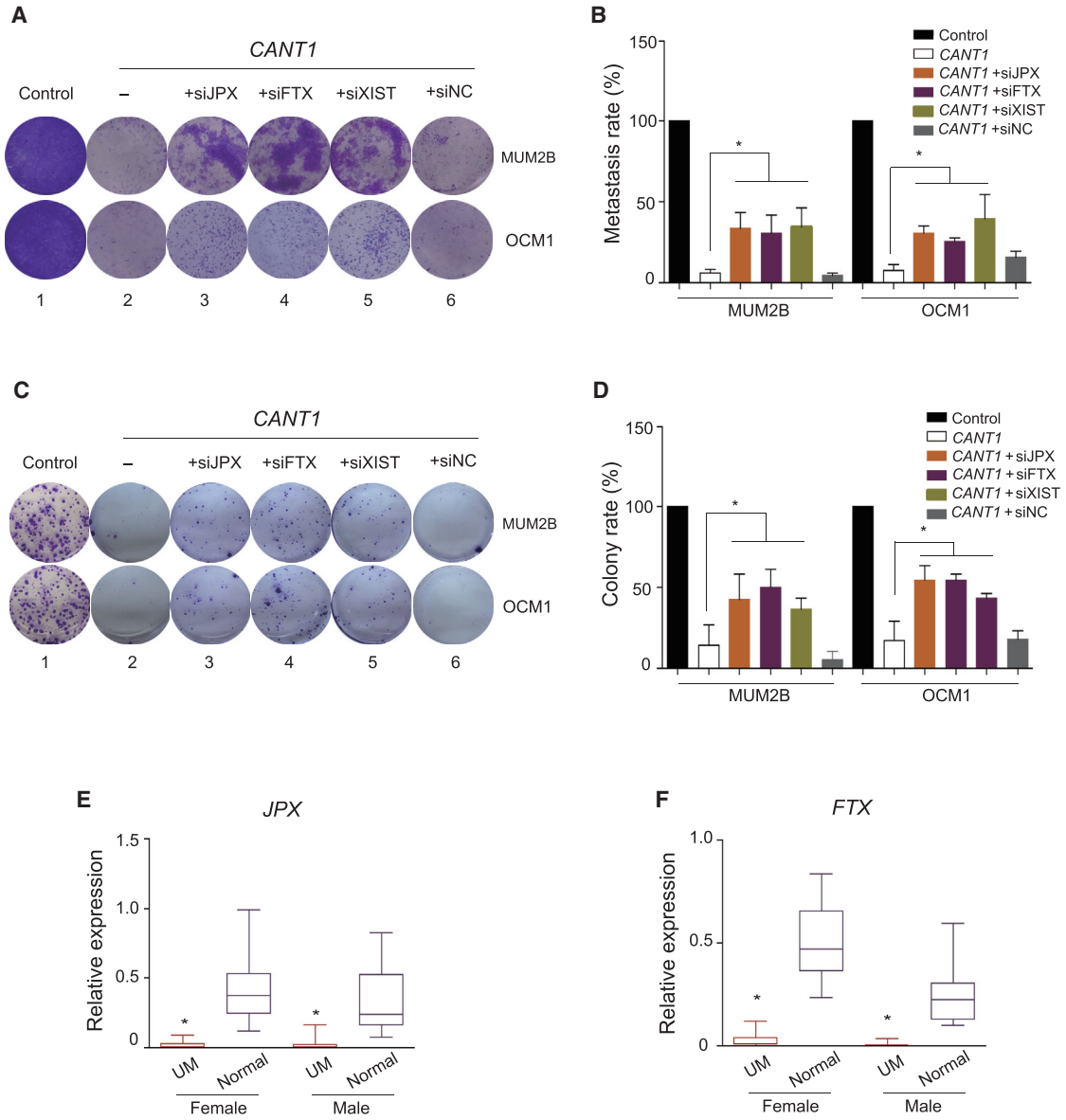

Figure 5. Role of the *CANT1*-Guided Cascade in UM

(A) A transwell assay was performed to estimate the migration of *CANT1*-expressing UM cells, including MUM2B and OCM1 cells, after siRNA treatment. Wild-type UM cells served as a control. The dash represents *CANT1*-expressing cells without siRNA, and these cells and siNC were used as control groups in this assay. (B) The absorbance values at a wavelength of 630 nm of stained migrated cells at day 3 were obtained to calculate the metastasis rate. The value of the control group was set to 100%. All of the experiments were performed in triplicate, and the relative metastasis rates are shown as mean ± SEM. *$p < 0.05$. (C) A colony formation assay was performed to assess tumor growth in *CANT1*-expressing UM cells after siRNA silencing. (D) Quantification of visible colonies. The colony number of the control group was set to 100%. All of the experiments were performed in triplicate, and the relative colony formation rates are shown as mean ± SEM. *$p < 0.05$. (E and F) Real-time PCR examination of *JPX* (E) and *FTX* (F) expression in UM tissues (12 female and 5 male subjects). Normal uveal tissues (7 female and 5 male subjects) were used as a control. The relative values are normalized to the *GAPDH* expression level and are presented as mean ± SEM. *$p < 0.05$.

changed at the *JPX* and *FTX* promoter regions after *CANT1* or *CANT-S* overexpression. Through a DNA quantitative chromatin immunoprecipitation (ChIP) assay, we found that H3K4 methylation at the *JPX* promoter was significantly increased after *CANT1* overexpression in two UM cell lines (Figure 7A, site a, left, *CANT1* column). We also found that H3K4 methylation of the *JPX* promoter was activated in *CANT1-S*-expressing MUM2B (Figure 7A, site a, left, *CANT1-S* column) and OCM1 cells (Figure 7B, site a, left, *CANT1-S* column). Similarly, we detected H3K4 methylation at the *FTX* promoter in *CANT1*-expressing UM cells (Figures 7C and 7D, site c, left, *CANT1* column).

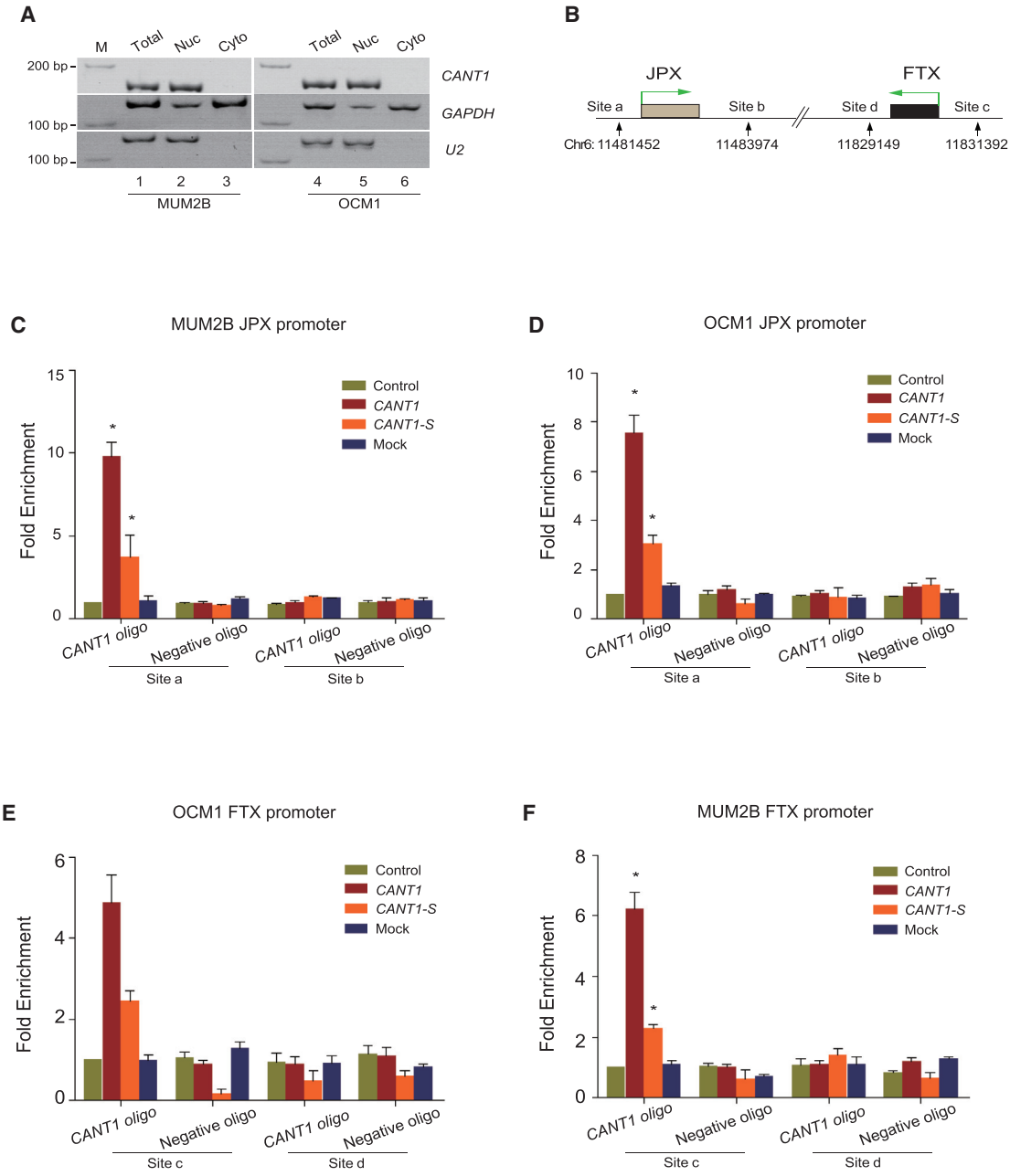

Figure 6. *CANT1* Binds to the Promoter of Its Targets

(A) Cellular localization of *CANT1* in MUM2B and OCM1 cells. *GAPDH* was used as a cytoplasmic positive control, and U2 was used as a nuclear positive control. (B) Schematic of sites in the *JPX* and *FTX* promoter detecting using the ChOP assay. (C and D) Real-time PCR examination of the binding of *CANT1* to the *JPX* promoter through the ChOP assay. *CANT1* oligo indicates the biotinylated antisense oligonucleotides against the *CANT1* lncRNA. Negative oligo indicates the scramble oligonucleotides and was used as a negative control in the ChOP assay. The value obtained for untreated UM cells was set to 1. (E and F) Quantification of the binding of *CANT1* to the *FTX* promoter in ChOP assay by real-time PCR. All of the experiments were performed in triplicate and are presented as mean ± SEM. *$p < 0.05$. The value obtained for untreated UM cells was set to 1.

We also found a similar positive trend of H3K4 methylation at the *FTX* promoter in *CANT1-S*-enriched UM cells (Figures 7C and 7D, site c, left, *CANT1-S* column). Taken together, these results demonstrated that either full-length *CANT1* or the short fragment *CANT1-S* controls the expression of *JPX* and *FTX* by promoting histone H3K4 methylation at their promoter regions.

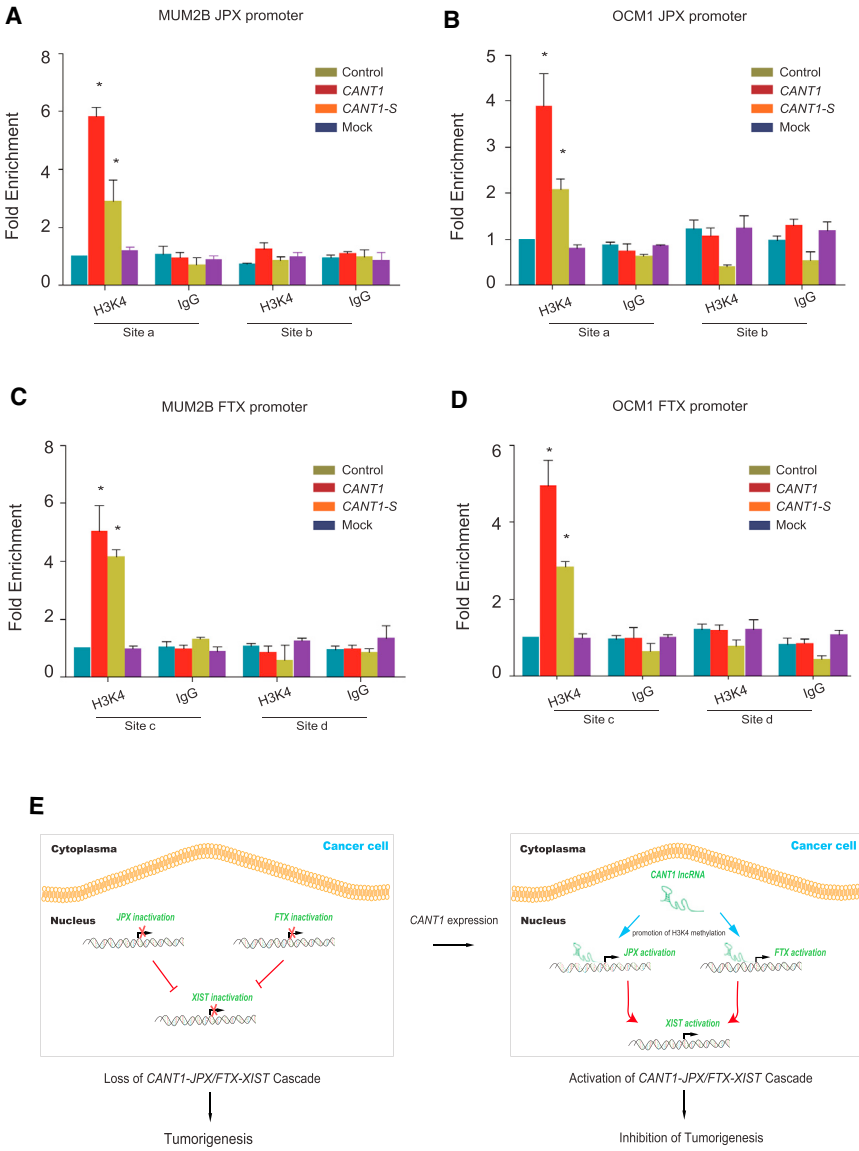

Figure 7. *CANT1* Modulates a Non-coding Cascade by Promoting H3K4 Methylation

(A and B) Real-time PCR examination of histone H3K4 tri-methylation changes in the *JPX* promoter upon *CANT1* expression in MUM2B (A) and OCM1 (B) cells. IgG was used as a negative control. The value obtained for untreated UM cells was set to 1. All of the experiments were performed in triplicate and are presented as mean ± SEM. *$p < 0.05$. (C and D) A real-time PCR assay was performed to quantify the H3K4 tri-methylation modifications in the *FTX* (C and D) promoters upon *CANT1* expression. The value obtained for untreated UM cells was set to 1. All of the experiments were performed in triplicate, and the relative values were normalized against the input values and are presented as mean ± SEM. *$p < 0.05$. (E) Schematic of the *CANT1*-guided non-coding cascade. The expression of *CANT1* lncRNA is inactivated in parental cancer cells, and these cells present a loss of the *CANT1*-guided non-coding cascade (left). After the expression of nuclear *CANT1*, *CANT1* recognizes and binds to the *JPX* and *FTX* promoters to promote H3K4 tri-methylation modifications and re-activate *JPX* and *FTX* expression. This activation relays the signal to *XIST*, completing an integrated long non-coding cascade that inhibits tumor growth and metastasis in UM. The black arrows represent activation.

DISCUSSION

lncRNAs are considered indispensable and important factors of epigenetic regulation and can play markedly different functional roles depending on the situation. Indeed, lncRNAs can mainly act via *cis* and *trans* regulatory functions. The *cis*-acting lncRNAs are restricted to the site of their synthesis and directly act on one or several linked, generally contiguous genes on the same chromosome.[7] In contrast, the *trans*-acting RNAs diffuse from their site of synthesis and affect many genes at great distances, including on other chromosomes. Both *cis*- and *trans*-acting lncRNAs can participate in tumorigenesis by modulating cell growth, migration, cycle or apoptosis in various cancers.[10,25–27] In this study, we report a novel isoform of *CASC15*, named *CASC15-New-Transcript 1* (*CASC15-NT1* or *CANT1*), that acts as a necessary tumor suppressor to modulate UM tumorigenesis through an lncing cascade that includes *JPX*, *FTX*, and *XIST* (Figure 7E).

It should be emphasized that the reported length of the *CASC15* lncRNA (formerly called *LINC00340*) is 1,904 bp and includes 12 exons.[18] Similarly, GENCODE annotations also predict six putative full-length transcripts ranging from 1,288–4,461 bp. In this study, however, we identified the *CANT1* lncRNA, a novel *CASC15* isoform derived from chromosome 6p22.3 that spans 1,114 bp in length and contains seven exons. *CASC15* has been confirmed to serve as a tumor suppressor in neuroblastoma,[16] but it also serves as a oncogene in the progression of cutaneous melanoma.[18] Because the etiology of UM is markedly different from that of cutaneous melanoma, it is not surprising that we found that *CANT1* lncRNA serves as the tumor suppressor that influences the properties of UM.

It also should be explained that *CANT1* is both exist in male and female normal uveal tissues in this study. Although downstream target of *CANT1*, *XIST* lncRNA, is a classic female-specific *cis*-acting lncRNA involved in XCI,[28] it does not suggest that UM tumorigenesis has a tight association with gender. Because tumorigenesis is a very complicated process with multiple causes, it is not surprising that female-specific *XIST* is theoretically involved in tumor initiation regardless of gender. For instance, in male-derived cancer (seminomatous testicular germ cell tumors [TGCTs]), *XIST* appears to be overexpressed, which is an unexpected finding,[29] and acts as an oncogene for TGCTs.[30] It also should be noted that the UM is caused by

complicated process accompanied by multiple defects,[5] *CANT1*-guided *XIST* pathway identified in this study is an alternative explanation for UM tumorigenesis regardless of gender. On the other hand, in normal development, unknown pathways or factors are likely to be involved, so further studies should also be focused on the unidentified function of *CANT1* in the development of the uvea.

It has been reported that *XIST* acts as an important inactivator of X chromosome in early human development. At this stage, *XIST* will recruit to the X chromosome to silence genes on the X chromosome, and *XIST* has a concentrated distribution, presenting as a single spot,[31] but a facultative heterochromatin is formed and gene repression becomes stable, *XIST* has dispersed organization, and XCI is independent of *XIST*.[32] In this study, FISH data show that *XIST* appears in a dispersed distribution, indicating that *XIST* merely expresses but may not be involved in inactivation of the X chromosome in *CANT1*-expressed UM cells. It should also be noted that OCM1 and MUM2B cells originated from female donors, and the reasons underlying weak expression of *XIST* in these two UM cells remain unclear. Therefore, it would be of great interest to focus on the identification of unknown mechanisms to better understand the regulation of *XIST* expression in UM.

It has been reported that in the mouse XCI, an lncRNA cluster containing *Jpx* and *Ftx* is associated with *XIST* regulation.[33] *Jpx* is a *Xist* regulator found approximately 10 kb upstream of *Xist*.[34,35] A recent study found that *Jpx* could compete with CTCF for binding to the *Xist* promoter and that activation of *Xist* expression occurs when *Jpx* is enriched in mouse differentiated cells.[35] *Ftx*, another well-conserved lncRNA, is also known as a *Xist* regulator during development in the mouse. *Ftx* deletion leads to a decrease in *Xist* expression.[34,36] Nonetheless, our results provide the first suggestion that human *XIST* expression is highly dependent on the mediation of *CANT1* in UM. Thus far, we still cannot rule out the possibility that other factors might be involved in the regulation of *XIST* expression in human UM cells. Therefore, it would be of great interest to focus on the identification of more factors to better understand the basis of *CANT1*-guided *XIST* expression in UM. On the other hand, as a downstream target of *JPX* or *FTX*, it is not surprising that knockdown of *XIST* does not produce a greater reversal effect than *JPX* or *FTX*, suggesting that other unidentified factors may also serve as necessary downstream targets of *JPX* or *FTX*. Future studies are needed to determine those factors, which may enhance the restoring efficiency of tumor-forming ability by silencing their expression simultaneously.

The exact mechanism underlying the transcriptional regulation of *JPX* or *FTX* remains unclear. Our study provides the first demonstration that *CANT1* modulates *JPX* or *FTX* transcription by initiating H3K4 methylation at their promoter. Most intriguingly, we also clearly indicated that *JPX* or *FTX*, as important regulatory non-coding molecules in XCI, function as necessary tumor suppressors that significantly inhibit malignant UM progression. Our findings redirect the attention given to well-known lncRNAs from the classical fields toward their emerging roles in the cancer field and unveil promising lncRNA targets that could be used for the diagnosis and treatment of cancers.

In most contexts, the genes targeted by an lncRNA are expected to be protein-coding genes. For example, the *ANRIL* lncRNA recruits PRC2 to silence KLF2 and P21 and thereby drive tumorigenesis.[37] The *MALAT1* lncRNA binds to the tumor suppressor SFPQ to release the proto-oncogene PTBP2 from the SFPQ/PTBP2 complex and thereby promote cell growth and metastasis.[38] However, the target of *CANT1* is not a coding protein but rather the nuclear *CANT1*-mediated lncing cascade, which serves as a contextual non-coding hinge to modulate tumor growth and metastasis in UM. Our proposed "lncing cascade" appears to be a special "relay race" of non-coding molecules in which the key players are not classical proteins but multifunctional lncRNAs. The biological signal is considered a relay baton, which is passed from one to another lncRNA to accomplish the final objective. Any interruption of lncing cascade during the relay will block the signal transduction pathway and affect tumorigenesis. Because many lncRNAs exist in various tumors, this "lncing-cascade renewal" anti-tumor strategy in UM also provides an alternative therapeutic approach for other cancers.

MATERIALS AND METHODS

Cell Culture

The human HDF, MUM2B, OCM1, OCM1A, OM431, SP6.5, and 293T cell lines were cultured in DMEM (GIBCO) supplemented with 10% certified heat-inactivated fetal bovine serum (FBS; GIBCO), penicillin (100 U/mL), and streptomycin (100 μg/mL) at 37°C in a humidified 5% CO_2 atmosphere. ARPE19 cells were cultured in DMEM/F12 medium (GIBCO), and 92.1 cells were cultured in RPMI 1640 medium (GIBCO). FPC1 cells were obtained as follows: sterile uveal tissue from a 30-year-old woman was cut into pieces and then digested in 0.1% collagenase A (GIBCO) for 18 hr at 37°C; the pieces were then pipetted from the turbid liquid to PBS without Ca^{2+} and Mg^{2+}; after filtration through a 100 μm pore size filter, the cell-containing solutions were centrifuged for 5 min; and after the supernatant was discarded, the pellet was resuspended in 10% FBS DMEM to yield a single-cell suspension. The cells were seeded at a density of $1 \times 10^5/cm^2$ and cultured as described above.

RT-PCR and Real-Time qPCR

Total RNA from cells and tissues was extracted using the TRIzol Reagent (GIBCO), and cDNA was synthesized using the PrimeScript RT-PCR Kit (Takara Bio). RT-PCR was performed using the Premix Ex Taq reagent (Takara Bio), and real-time PCR was performed using the SYBR Select Master Mix (Applied Biosystems) and an ABI 7500 real-time PCR system (Applied Biosystems).

RACE Assay

The RACE assay was performed as previously described.[39] The first-strand cDNA was synthesized using the MMuLV First-Strand cDNA Synthesis Kit (BBI), and PCR was performed using the LA Taq DNA polymerase (Takara Bio).

Plasmid Construction

CANT1 was cloned using the KOD-Plus-Neo DNA polymerase (TOYOBO) and ARPE19 cDNA with the following procedure: incubation at 94°C for 2 min followed by 40 cycles of denaturation at 98°C for 10 s, annealing at the optimal temperature for 30 s, and extension at 68°C for 1 min for extension and a single final extension at 68°C for 7 min. The cloning primers were designed with BamHI and EcoRI sites. The sequence was then cloned into the pCDH-CMV-MCS-EF1-Puro lentivirus vector (System Biosciences).

Lentivirus Packaging and Generation of Stable Cell Lines

The Lipofectamine 2000 reagent (Invitrogen) incubated with Opti-MEM I Reduced Serum Medium (GIBCO) was used to transfect 239T cells with 3 μg of the PCMV-CANT1 plasmid, 3 μg of the pMD2.D plasmid, and 6.0 μg of the PsPax plasmid. Six hours after transfection, the medium was replaced with 10 mL of fresh medium. The supernatants containing viruses were collected at 48 and 72 hr. The virus-containing solution was filtered through a 0.45 μm cellulose acetate filter, concentrated with an Amicon Ultra-15 Centrifugal Filter Unit (Millipore) at 3,000 rpm and 4°C for 30 min, aliquoted, and frozen at −80°C for long-term storage.

Twenty-four hours prior to transduction, tumor cells were seeded at 1.0×10^5 cells per well in a six-well plate. The medium was replaced with a virus-containing supernatant supplemented with 10 ng/mL polybrene (Sigma-Aldrich). After 48 hr, the medium was replaced with fresh medium. Selection was performed by incubating with 4 μg/mL puromycin (InvivoGen) for 2 weeks. Colonies were selected and expanded for further analyses.

Transwell Assay

The migratory ability of the cells was evaluated using a 24-well transwell system with 8 μm pore size polycarbonate filters (Millipore). The upper compartment contained 10,000 cells suspended in the appropriate medium supplemented with 2% FBS, and the lower compartment contained 10% FBS. After 2 days of incubation at 37°C, the transwell system was stained with 0.25% crystal violet. The cells on the inner side of the transwell were removed by scrubbing, and the cells on the outer side were photographed. The crystal violet stain was washed from the migrated cells using 100 μL of 33% acetic acid. The absorbance values of the liquid at 630 nm were determined using a microplate reader.

Colony Formation Assay

A volume of 1 mL of 0.6% agar complete medium was spread in each well of a six-well plate to obtain the bottom layer, and 5,000 cells were resuspended in 1.0 mL of 0.3% agar complete medium and seeded into the upper layer. The cells were cultured with 300 μL of complete medium for 3–4 weeks. The colonies in soft agar were stained with 0.005% crystal violet and then photographed.

Xenograft Model

The animal experiments were approved by the Shanghai JiaoTong University Animal Care and Use Committee and conducted following the animal policies of the Shanghai JiaoTong University in accordance with the guidelines established by the National Health and Family Planning Commission of China. The cells were harvested by trypsinization and washed twice with PBS (GIBCO). The cells (5×10^6) in 100 μL of PBS were then injected subcutaneously into the right flank of 4-week-old male nude mice. The length and the width of the tumors were measured twice a week until 21 days after injection. The size of the tumors was calculated using the formula length × width × width/2. The tumors were excised after euthanasia, and total RNA was extracted for subsequent examination.

Genome-wide cDNA Array

The Affymetrix PrimeView Human Gene Expression Array was used in this experiment. Total RNA was extracted using the TRIzol Reagent and quantified using a NanoDrop ND-2000 spectrophotometer (Thermo Scientific). RNA integrity was assessed using an Agilent Bioanalyzer 2100 (Agilent Technologies). Sample labeling, microarray hybridization, and washing were performed on the basis of the manufacturer's standard protocols. Briefly, total RNA was transcribed into double-stranded cDNA, and the cDNA was then labeled with biotin. The labeled cDNAs were hybridized onto the microarray. After washing and staining, the arrays were scanned using an Affymetrix Scanner 3000 (Affymetrix). The Affymetrix GeneChip Command Console (version 4.0; Affymetrix) was used to analyze the array images and obtain the raw data. Genespring software (version 12.5; Agilent Technologies) was used to perform the basic analyses of the raw data. First, the raw data were normalized using the RMA algorithm. The differentially expressed genes were then identified using Student's t test with a p value less than 0.05, and genes presenting a 2-fold change in expression were considered differentially regulated by the *CANT1* lncRNA.

Small Interfering RNA

The small interfering RNAs (siRNAs) were designed and synthesized by Biomics. A total of 1×10^5 PCMV-CANT1 cells were seeded in each well of a six-well plate and transfected with 125 pmol of siRNA (tested gene or negative control) using Lipofectamine 2000 in Opti-MEM I Reduced Serum Medium (GIBCO). Six hours after transfection, the supernatant was replaced by fresh complete medium, and 48 hr after transfection, the cells were harvested in TRIzol for RNA isolation. Twenty-four hours after transfection, the cells were harvested by trypsinization and used for tumor assays.

Cytoplasmic and Nuclear RNA Isolation

Cytoplasmic and nuclear RNA was extracted using the Fisher BioReagents SurePrep Nuclear or Cytoplasmic RNA Purification Kit (Thermo Fisher) according to the manufacturer's instructions. The RNA was reverse-transcribed to cDNA and used for RT-PCR.

RNA FISH

The RNA FISH assay was performed as previously described.[8] Briefly, cells were fixed with 4% formaldehyde/10% acetic acid and stored overnight in 70% ethanol, and fluorescence-labeled single-strand probes were synthesized (Empire Genomics; http://www.empiregenomics.com/shop/XIST-FISH-Probe.html) and were hybridized. To increase

the stability of RNA foci, RNA signals were detected with a tyramide-Alexa Fluor 488 signal amplification kit (Invitrogen). After labeling, fluorescence was detected using a microscope (BX41; Olympus). Optical sections of 0.5 μm were collected with SlideBook 5.0 (Intelligent Imaging Innovations).

ChOP

The ChOP assay was performed as previously described.[8,13] Briefly, the cells were fixed with 1% formaldehyde (Sigma-Aldrich) and centrifuged at 3,000 rpm for 15 min. The pellet was suspended in 300 μL of buffer A (3 mM $MgCl_2$, 10 mM Tris-HCl [pH 7.4], 10 mM NaCl, and 0.5% NP-40) and incubated for 5 min on ice. The nuclei were resuspended in 150 μL of buffer B (50 mM Tris-HCl [pH 7.9], 10 mM EDTA, 0.2 mM PMSF, 1% SDS, protease inhibitors [Roche], and 100 U/mL RNase [Ambion]) and incubated on ice for 10 min. A volume of 150 μL of buffer C (15 mM Tris-HCl [pH 7.9], 150 mM NaCl, 1 mM EDTA, 1% Triton X-100, 0.2 mM PMSF, protease inhibitors, and 100 U/mL RNase_ was added, and the samples were sonicated (10 s on, 15 s off, output 30%, 4 min). After centrifugation, 150 μL aliquots of sonicated chromatin was combined with 100 pmol of either biotinylated antisense oligonucleotides against the target RNA or biotinylated control oligonucleotides, incubated at a proper annealing temperature for 5 min and then slowly cooled to room temperature. A 50 μL volume of beads was used to capture the biotinylated DNA/RNA complexes for 25 min at room temperature with gentle rotation. After three washes, 150 μL of diethyl pyrocarbonate (DEPC) water was used for elution at 70°C for 5 min. After crosslink reversal and purification, the samples were ready for PCR.

A TaqMan assay using the ABI 7500 Real-Time PCR System was performed to detect the quality of the *CANT1* pulled down by Dynabeads MyOne Streptavidin C1 beads. Primers and probes labeled at their 5′ and 3′ ends with FAM and black hole quencher-1 (BHQ-1) or minor groove binder (MGB) were designed to target *CANT1*. The amplification reactions were optimized individually for all of the probes and associated primers. Each reaction was conducted in a total volume of 10 μL consisting of 0.6 μL of 25 mM $MgCl_2$, 0.25 μL of 10 mM dinucleotide triphosphates (dNTPs), 2 μL of 5 × Q buffer, 0.25 μL of each 10 μM primer, 0.1 μL of the TaqMan probe, 0.1 μL of 5 U/μL Hotstar, 0.1 μL of the reference ROX dye, and 4 μL of the template.

ChIP

The ChIP assay was performed as previously described.[8,13] The cells were fixed with 1% formaldehyde and centrifuged, and the pellets were resuspended with ChIP lysis buffer (50 mM Tris-HCl [pH 8.0]), incubated for 10 min on ice, and then sonicated (10 s on, 15 s off, output 30%, 4 min). The supernatant was collected into a new tube, and 5 μg of antibody (H3K4 [Cell Signaling Technology], H3K9, H3K27, H3K36, and IgG [Abcam]) was added. The mixture was then incubated overnight at 4°C, and 60 μL of Pure Proteome Protein A and Protein G Magnetic Beads (Millipore) was used to pull down the DNA-protein-antibody complexes at 4°C for 6 hr. The DNA complexes were eluted using 0.2 M glycine. After crosslink reversal and purification, the samples were ready for PCR.

Real-time PCR was performed using an ABI Prism 7500 Sequence Detection System (Applied Biosystems) and the Power SYBR Green PCR Master Mix (Applied Biosystems). The standard PCR conditions were the following: 50°C for 15 min, 94°C for 2 min, 40 cycles of 94°C for 20 s, annealing at the optimal annealing temperature for 30 s, extension at 72°C for 35 s, and fluorescence signal detection at 86°C.

Statistical Analysis

All of the experiments were performed in triplicate, and the data are expressed as mean ± SEM. For comparison of relative expression, control group normally set as 1 or 100% as compared with other treated groups as previously described.[13,15] The comparative threshold cycle method was applied to the quantitative real-time PCR assay data according to the ΔΔ threshold cycle method. The differences between two groups were analyzed using the unpaired two-sided Student's t test. A p value less than 0.05 was considered to indicate statistical significance, and these differences are indicated with asterisks, as described in the figure legends.

SUPPLEMENTAL INFORMATION

Supplemental Information includes four figures and three tables and can be found with this article online at http://dx.doi.org/10.1016/j.ymthe.2017.02.016.

AUTHOR CONTRIBUTIONS

Y.X., X.W., X.D., J.F., and P.C. designed and performed the experiments and drafted the manuscript. R.J. was responsible for sample collection and data analysis. S.G. and G.Q. discussed and revised the manuscript. H.Z. and X.F. wrote and approved the manuscript. All authors approved this manuscript.

CONFLICTS OF INTEREST

The authors declare no conflict of interest.

ACKNOWLEDGMENTS

This work was supported by the National Natural Science Foundation of China (grants 31470757, 81372469, U1432117, and 81602525), the Scientific Research Program of the National Health and Family Planning Commission of China (201402014), the Program for Professor of Special Appointment (Eastern Scholar) at the Shanghai Institutions of Higher Learning (1410000159), the SMC-ChenXing Yong Scholar Program (2014, Class B), the Shanghai Municipal Education Commission-Gaofeng Clinical Medicine Grant (20161317), the Science and Technology Commission of Shanghai (grants 14JC1404100, 14JC1404200, and 14430723100), and the Outstanding Yong Scholar Grant of Shanghai JiaoTong University School of Medicine (16XJ11002). The funders had no role in the study design, data collection and analysis, decision to publish, or preparation of the manuscript.

REFERENCES

1. Gomez, D., Wetherill, C., Cheong, J., Jones, L., Marshall, E., Damato, B., Coupland, S.E., Ghaneh, P., Poston, G.J., Malik, H.Z., and Fenwick, S.W. (2014). The Liverpool uveal melanoma liver metastases pathway: outcome following liver resection. J. Surg. Oncol. *109*, 542–547.

2. Onken, M.D., Worley, L.A., Ehlers, J.P., and Harbour, J.W. (2004). Gene expression profiling in uveal melanoma reveals two molecular classes and predicts metastatic death. Cancer Res. *64*, 7205–7209.
3. Abdel-Rahman, M.H., Christopher, B.N., Faramawi, M.F., Said-Ahmed, K., Cole, C., McFaddin, A., Ray-Chaudhury, A., Heerema, N., and Davidorf, F.H. (2011). Frequency, molecular pathology and potential clinical significance of partial chromosome 3 aberrations in uveal melanoma. Mod. Pathol. *24*, 954–962.
4. Harbour, J.W., Onken, M.D., Roberson, E.D., Duan, S., Cao, L., Worley, L.A., Council, M.L., Matatall, K.A., Helms, C., and Bowcock, A.M. (2010). Frequent mutation of BAP1 in metastasizing uveal melanomas. Science *330*, 1410–1413.
5. Field, M.G., and Harbour, J.W. (2014). Recent developments in prognostic and predictive testing in uveal melanoma. Curr. Opin. Ophthalmol. *25*, 234–239.
6. Ledford, H. (2008). Language: disputed definitions. Nature *455*, 1023–1028.
7. Lee, J.T. (2012). Epigenetic regulation by long noncoding RNAs. Science *338*, 1435–1439.
8. Zhang, H., Zeitz, M.J., Wang, H., Niu, B., Ge, S., Li, W., Cui, J., Wang, G., Qian, G., Higgins, M.J., et al. (2014). Long noncoding RNA-mediated intrachromosomal interactions promote imprinting at the Kcnq1 locus. J. Cell Biol. *204*, 61–75.
9. Zhang, Y., Xia, J., Li, Q., Yao, Y., Eades, G., Gernapudi, R., Duru, N., Kensler, T.W., and Zhou, Q. (2014). NRF2/long noncoding RNA ROR signaling regulates mammary stem cell expansion and protects against estrogen genotoxicity. J. Biol. Chem. *289*, 31310–31318.
10. Gutschner, T., Hämmerle, M., Eissmann, M., Hsu, J., Kim, Y., Hung, G., Revenko, A., Arun, G., Stentrup, M., Gross, M., et al. (2013). The noncoding RNA MALAT1 is a critical regulator of the metastasis phenotype of lung cancer cells. Cancer Res. *73*, 1180–1189.
11. Okugawa, Y., Toiyama, Y., Hur, K., Toden, S., Saigusa, S., Tanaka, K., Inoue, Y., Mohri, Y., Kusunoki, M., Boland, C.R., and Goel, A. (2014). Metastasis-associated long non-coding RNA drives gastric cancer development and promotes peritoneal metastasis. Carcinogenesis *35*, 2731–2739.
12. He, Y., Meng, X.M., Huang, C., Wu, B.M., Zhang, L., Lv, X.W., and Li, J. (2014). Long noncoding RNAs: Novel insights into hepatocelluar carcinoma. Cancer Lett. *344*, 20–27.
13. Fan, J., Xing, Y., Wen, X., Jia, R., Ni, H., He, J., Ding, X., Pan, H., Qian, G., Ge, S., et al. (2015). Long non-coding RNA ROR decoys gene-specific histone methylation to promote tumorigenesis. Genome Biol. *16*, 139.
14. Xu, S., Wang, H., Pan, H., Shi, Y., Li, T., Ge, S., Jia, R., Zhang, H., and Fan, X. (2016). ANRIL lncRNA triggers efficient therapeutic efficacy by reprogramming the aberrant INK4-hub in melanoma. Cancer Lett. *381*, 41–48.
15. Zhang, H., Wang, H., Zhang, J., Qian, G., Niu, B., Fan, X., Lu, J., Hoffman, A.R., Hu, J.F., and Ge, S. (2009). Enhanced therapeutic efficacy by simultaneously targeting two genetic defects in tumors. Mol. Ther. *17*, 57–64.
16. Russell, M.R., Penikis, A., Oldridge, D.A., Alvarez-Dominguez, J.R., McDaniel, L., Diamond, M., Padovan, O., Raman, P., Li, Y., Wei, J.S., et al. (2015). CASC15-S is a tumor suppressor lncRNA at the 6p22 neuroblastoma susceptibility locus. Cancer Res. *75*, 3155–3166.
17. Capasso, M., Diskin, S., Cimmino, F., Acierno, G., Totaro, F., Petrosino, G., Pezone, L., Diamond, M., McDaniel, L., Hakonarson, H., et al. (2014). Common genetic variants in NEFL influence gene expression and neuroblastoma risk. Cancer Res. *74*, 6913–6924.
18. Lessard, L., Liu, M., Marzese, D.M., Wang, H., Chong, K., Kawas, N., Donovan, N.C., Kiyohara, E., Hsu, S., Nelson, N., et al. (2015). The CASC15 long intergenic noncoding RNA locus is involved in melanoma progression and phenotype switching. J. Invest. Dermatol. *135*, 2464–2474.
19. Harrow, J., Denoeud, F., Frankish, A., Reymond, A., Chen, C.K., Chrast, J., Lagarde, J., Gilbert, J.G.R., Storey, R., Swarbreck, D., et al. (2006). GENCODE: producing a reference annotation for ENCODE. Genome Biol. *7* (*Suppl 1*), S4.
20. Ørom, U.A., Derrien, T., Beringer, M., Gumireddy, K., Gardini, A., Bussotti, G., Lai, F., Zytnicki, M., Notredame, C., Huang, Q., et al. (2010). Long noncoding RNAs with enhancer-like function in human cells. Cell *143*, 46–58.
21. Yildirim, E., Kirby, J.E., Brown, D.E., Mercier, F.E., Sadreyev, R.I., Scadden, D.T., and Lee, J.T. (2013). Xist RNA is a potent suppressor of hematologic cancer in mice. Cell *152*, 727–742.
22. Sinclair, A.H., Berta, P., Palmer, M.S., Hawkins, J.R., Griffiths, B.L., Smith, M.J., Foster, J.W., Frischauf, A.M., Lovell-Badge, R., and Goodfellow, P.N. (1990). A gene from the human sex-determining region encodes a protein with homology to a conserved DNA-binding motif. Nature *346*, 240–244.
23. Jacob, R.R., Saxena, R., and Verma, I.C. (2015). Noninvasive diagnosis of fetal gender: utility of combining DYS14 and SRY. Genet. Test. Mol. Biomarkers *19*, 505–511.
24. Sekido, R., and Lovell-Badge, R. (2008). Sex determination involves synergistic action of SRY and SF1 on a specific Sox9 enhancer. Nature *453*, 930–934.
25. Gupta, R.A., Shah, N., Wang, K.C., Kim, J., Horlings, H.M., Wong, D.J., Tsai, M.C., Hung, T., Argani, P., Rinn, J.L., et al. (2010). Long non-coding RNA HOTAIR reprograms chromatin state to promote cancer metastasis. Nature *464*, 1071–1076.
26. Tang, L., Zhang, W., Su, B., and Yu, B. (2013). Long noncoding RNA HOTAIR is associated with motility, invasion, and metastatic potential of metastatic melanoma. BioMed Res. Int. *2013*, 251098.
27. Feldstein, O., Nizri, T., Doniger, T., Jacob, J., Rechavi, G., and Ginsberg, D. (2013). The long non-coding RNA ERIC is regulated by E2F and modulates the cellular response to DNA damage. Mol. Cancer *12*, 131.
28. Zhao, J., Sun, B.K., Erwin, J.A., Song, J.J., and Lee, J.T. (2008). Polycomb proteins targeted by a short repeat RNA to the mouse X chromosome. Science *322*, 750–756.
29. Kawakami, T., Okamoto, K., Sugihara, H., Hattori, T., Reeve, A.E., Ogawa, O., and Okada, Y. (2003). The roles of supernumerical X chromosomes and XIST expression in testicular germ cell tumors. J. Urol. *169*, 1546–1552.
30. Kawakami, T., Okamoto, K., Ogawa, O., and Okada, Y. (2004). XIST unmethylated DNA fragments in male-derived plasma as a tumour marker for testicular cancer. Lancet *363*, 40–42.
31. McHugh, C.A., Chen, C.K., Chow, A., Surka, C.F., Tran, C., McDonel, P., Pandya-Jones, A., Blanco, M., Burghard, C., Moradian, A., et al. (2015). The Xist lncRNA interacts directly with SHARP to silence transcription through HDAC3. Nature *521*, 232–236.
32. Wutz, A. (2011). Gene silencing in X-chromosome inactivation: advances in understanding facultative heterochromatin formation. Nat. Rev. Genet. *12*, 542–553.
33. Tian, D., Sun, S., and Lee, J.T. (2010). The long noncoding RNA, Jpx, is a molecular switch for X chromosome inactivation. Cell *143*, 390–403.
34. Chureau, C., Prissette, M., Bourdet, A., Barbe, V., Cattolico, L., Jones, L., Eggen, A., Avner, P., and Duret, L. (2002). Comparative sequence analysis of the X-inactivation center region in mouse, human, and bovine. Genome Res. *12*, 894–908.
35. Sun, S., Del Rosario, B.C., Szanto, A., Ogawa, Y., Jeon, Y., and Lee, J.T. (2013). Jpx RNA activates Xist by evicting CTCF. Cell *153*, 1537–1551.
36. Chureau, C., Chantalat, S., Romito, A., Galvani, A., Duret, L., Avner, P., and Rougeulle, C. (2011). Ftx is a non-coding RNA which affects Xist expression and chromatin structure within the X-inactivation center region. Hum. Mol. Genet. *20*, 705–718.
37. Nie, F., Sun, M., Yang, J., Xie, M., Xu, T., Xia, R., Liu, Y.W., Liu, X.H., Zhang, E.B., Lu, K.H., and Shu, Y.Q. (2014). Long noncoding RNA ANRIL promotes non-small cell lung cancer cell proliferation and inhibits apoptosis by silencing KLF2 and P21 expression. Mol. Cancer Ther. *14*, 268–277.
38. Ji, Q., Zhang, L., Liu, X., Zhou, L., Wang, W., Han, Z., Sui, H., Tang, Y., Wang, Y., Liu, N., et al. (2014). Long non-coding RNA MALAT1 promotes tumour growth and metastasis in colorectal cancer through binding to SFPQ and releasing oncogene PTBP2 from SFPQ/PTBP2 complex. Br. J. Cancer *111*, 736–748.
39. Salehi-Ashtiani, K., Lin, C., Hao, T., Shen, Y., Szeto, D., Yang, X., Ghamsari, L., Lee, H., Fan, C., Murray, R.R., et al. (2009). Large-scale RACE approach for proactive experimental definition of C. elegans ORFeome. Genome Res. *19*, 2334–2342.